



## Magnetic memory and coupling between spin-canted and defect magnetism in hematite

Özden Özdemir<sup>1</sup> and David J. Dunlop<sup>1</sup>

Received 8 June 2006; revised 27 July 2006; accepted 15 August 2006; published 17 November 2006.

[1] Saturation isothermal remanent magnetization (SIRM) has been studied on submicron hematite powders with grain sizes between 0.12 and 0.52  $\mu\text{m}$  and on 2 to 5 mm natural hematite single crystals before and after zero-field cycling through the Morin transition ( $T_M$ ). SIRM cooling and warming curves for single-domain (SD) crystals are similar to those of multidomain (MD) hematites. Both have similar remanence losses at  $T_M$  (97–98% of the original SIRM), a similar defect moment below  $T_M$  (2–3% of initial SIRM), and similar memory (30–40% of initial SIRM). Regardless of grain size, higher SIRM memory ratios are associated with higher defect moments below  $T_M$ . In SD and MD hematites alike, room temperature magnetic memory seems to be an amplification of residual weak ferromagnetism that persists even at very low temperatures, much below  $T_M$ . Applying a strong field to initially demagnetized SD and MD hematites at 20 K produced a substantial SIRM, which spontaneously increased by a factor 10–28 upon crossing the transition at  $T_M$ . These observations imply that some spins do not participate in the general rotation from the ferromagnetic  $c$  plane to the antiferromagnetic  $c$  axis below  $T_M$ . The defect moment of these spins serves to restore preferred directions of spins and ferromagnetic domains during zero-field warming through the Morin transition and is thus responsible for the memory phenomenon. The existence of a weak ferromagnetic moment in antiferromagnetic hematite below  $T_M$  is also indicated by colloid patterns observed by Gallon. We propose that the mechanism of memory is clusters of spins pinned magnetoelastically by lattice defects. These spins rotate only partially out of the basal plane during cooling through  $T_M$ . Some basal plane anisotropy, also magnetoelastic in origin, must remain below  $T_M$  in order to explain the existence of low-temperature SIRM and also to guide spin nuclei into preferred orientations above  $T_M$  on rewarming through the transition in zero field.

**Citation:** Özdemir, Ö., and D. J. Dunlop (2006), Magnetic memory and coupling between spin-canted and defect magnetism in hematite, *J. Geophys. Res.*, 111, B12S03, doi:10.1029/2006JB004555.

### 1. Introduction

[2] Hematite is the ultimate magnetic oxide that forms in oxidizing environments like the surfaces of Earth and Mars. Although hematite is weakly magnetic compared to ferromagnetic oxides like magnetite and titanomagnetite, its natural remanent magnetization (NRM) is important in the paleomagnetic record. Even when hematite's NRM is secondary and undesirable, it is extremely persistent, both in nature and in the laboratory. In single-domain (SD) form, as crystals  $\leq 20 \mu\text{m}$  in size, its coercivities are typically many hundreds of mT, so that the NRM cannot be selectively removed by alternating field (AF) demagnetization. In either SD or multidomain (MD) form, the high Néel/ Curie temperature  $T_N = 680\text{--}690^\circ\text{C}$  and resulting high

unblocking temperatures make the NRM resistant to thermal demagnetization as well.

[3] Above the Morin transition, hematite is a canted antiferromagnet. The canted spin sublattices and resulting perpendicular net spontaneous magnetization  $M_s$ , lie in the crystallographic  $c$  plane, the basal plane of its rhombohedral crystals. Below the Morin transition at  $T_M = 250\text{--}260$  K, the spin sublattices rotate to the  $c$  axis and spin canting in theory disappears [Dzyaloshinsky, 1958; Moriya, 1960]. Yet Néel and Pauthenet [1952] had earlier shown the existence of a sizable magnetization below  $T_M$  in a large hematite crystal. Néel [1953] dubbed this the parasitic or defect magnetization. He first believed the “defect” was chemical: trace amounts of magnetite [Néel, 1949]. This cannot be the general explanation, because none of our fine- and coarse-grained hematites exhibits the magnetite Verwey transition around 120 K. Néel [1953] also mentions “defects of crystallization”, a more plausible explanation. Annealing, which reduces dislocation density, also reduces the defect moment [Dunlop, 1971] and suppresses domain structure below  $T_M$  [Gallon, 1968a].

<sup>1</sup>Department of Chemical and Physical Sciences, University of Toronto at Mississauga, Mississauga, Ontario, Canada.

**Table 1.** Low-Temperature Magnetic Properties of Submicron Hematites

Sample	$d$ , $\mu\text{m}$	$T_M$ , K	$R_{\text{SIRM}}$	$M_{\text{defect}}$ , kA/m
HH-1	0.135	252	0.394	0.0167
HH-2	$0.25 \pm 0.08$	228	0.392	0.0246
HH-3	$0.27 \pm 0.10$	254	0.384	0.0159
HH-4	0.33	255	0.386	0.0163
HH-5	$0.36 \pm 0.11$	230	0.367	0.0166
HH-6	$0.42 \pm 0.18$	246	0.35	0.0207
HMN-1	$0.35 \pm 0.12$	254	0.30	0.0101
HMN-2	0.45	254	0.35	0.017
HMH-1	$0.35 \pm 0.12$	252	0.275	0.0106
HMH-2	0.4	250	0.295	0.0123
HLP	$0.52 \pm 0.16$	248	0.321	0.0111
H1	$0.23 \pm 0.05$	243	0.298	0.0147
H2	$0.19 \pm 0.06$	241	0.274	0.0112
H3	$0.17 \pm 0.05$	243	0.318	0.0101
H4	$0.12 \pm 0.04$	241	0.312	0.0117

[4] The phenomenon of memory was investigated by *Haigh* [1957a, 1957b]. When a crystal of hematite is given a remanence and cycled in zero field through  $T_M$ , it loses much of its remanence in the cooling half cycle but regains a fraction of this in the heating half cycle, even though there is no field present to orient the memory remanence. Evidently something must be guiding the spin-canted magnetization into a particular easy direction in the  $c$  plane as it renucleates in warming through  $T_M$  and the only likely candidate is the defect magnetization surviving below  $T_M$ . In support of this view, memory decreases when the defect moment is partially annealed out [*Gallon*, 1968b].

[5] Recently, *Özdemir and Dunlop* [2005] discovered that room temperature remanence and the cooling half cycle are not essential to the memory phenomenon. They produced a saturation isothermal remanent magnetization (SIRM) in a large hematite crystal by applying a 2.5 T field at 20 K. This relatively small SIRM, a pure defect remanence, spontaneously increased by a factor  $\sim 25$  when warmed through  $T_M$ , preserving its direction in the process. Room temperature memory seems to be in essence an amplification of the defect remanence, the much stronger spin-canted magnetization passively following the direction of the defect remanence on warming through  $T_M$ —in effect, a magnetic transistor!

[6] Magnetic memory after low-temperature cycling has some practical relevance. Hematite is the commonest magnetic mineral on Mars' surface. It is identified by *Opportunity* and *Spirit's* Mössbauer and mini-TES spectrometers [*Squyres et al.*, 2004; *Christensen et al.*, 2004; *Klingelhöfer et al.*, 2004] as millimeter-sized spherules in ancient layered bedrocks [*Squyres and Knoll*, 2005; *Glotch and Christensen*, 2005]. Mars is a cold planet, with surface temperatures averaging  $\approx 220$  K. Surface and subsurface temperatures in parts of the planet cycle daily or seasonally through  $T_M$  in the zero present-day Martian field. Where surface temperatures are higher than  $T_M$  (250–260 K), the very stable magnetic memory of hematite could be a contributor to Martian magnetic anomalies.

[7] The purpose of the present study was to investigate further the memory phenomenon with a much larger set of SD and MD hematites. The first question to be answered is whether a larger defect remanence in general leads to a

larger memory. If so, what is the mechanism of coupling between the spin-canted and defect magnetizations?

## 2. Sample Characterization

[8] We made measurements on five sets of submicron SD hematites and on large MD single crystals from three localities. Samples HH1-6 are Pfizer hematite powders which were heated in air for 5 hours at 500°C to oxidize possible magnetic impurities such as maghemite or magnetite. Median particle sizes after the heat treatment were 0.135–0.42  $\mu\text{m}$  (Table 1). HMN and HMH hematites were produced by heating Pfizer acicular magnetite and maghemite, respectively, at 700°C in air for 19 hours. The heat treatment resulted in rounded grains with average lengths ranging from 0.35 to 0.45  $\mu\text{m}$ . Sample HLP contains acicular particles of average diameter 0.06  $\mu\text{m}$  and length 0.52  $\mu\text{m}$  prepared by heating synthetic Pfizer lepidocrocite. Samples H1-4 were obtained by heating cube-shaped magnetite crystals at 700°C in air for 18 hours.

[9] Grain size distributions for all the submicron hematites were measured with a Hitachi S4500 scanning electron microscope operated at 10 kV. X-ray analysis using a Siemens D5000 X-ray diffractometer with Co  $K\alpha$  radiation gave well-defined diffraction patterns characteristic of hematite, uncontaminated by other iron oxides (Figure 1).

[10] The natural single crystals of hematite are from Mount Wright, Québec, Canada; Rio Marina, Elba, Italy; and Bahia, Brazil. Sixteen smaller crystals (including a powder of smaller crystals: BRZ-2) cleaved from the parent hematite crystals were examined under a Nikon SMZ10 stereoscopic microscope (Table 2). The crystals are basal plane platelets with (0001) faces between 1 mm  $\times$  2 mm and 3.7 mm  $\times$  5.5 mm in size and thicknesses of 0.14–1.0 mm (Table 2). Scanning electron microscopy (Hitachi S570) linked with energy dispersive X-ray microanalysis (EDAX LZ-5) was carried out on representative crystals from each location. EDAX confirmed that the crystals are stoichiometric hematite with no significant impurities (Figure 2).

[11] The Néel temperature  $T_N$  was determined from high-field thermomagnetic curves measured with a vibrating-sample magnetometer (PMC micro-VSM). Figure 3 shows the temperature variation of high-field magnetization of natural single crystal QC-4. The  $M_s(T)$  curve of hematite is “blocky”, being almost temperature-independent between 20 and 500°C and decreasing strongly above 600°C.  $T_N$  ranged almost 20°C, from 679 to 696°C, averaging  $\approx 6^\circ\text{C}$  higher for the synthetic submicron hematites than for the natural crystals. These values are in the range of reported values of  $T_N$  measured on pure synthetic single crystals [*Chevallier*, 1951; *Freier et al.*, 1962; *Lielmezs and Chaklader*, 1965].

[12] Room temperature hysteresis loops were measured with a PMC micro-VSM. The maximum field of 1.5 T was not sufficient to saturate the magnetization of the submicron SD hematites. Their hysteresis loops did not close (Figure 4). Bulk coercive forces  $H_c$  ranging from 140 to 670 mT were determined from the unsaturated loops (Table 3) but the coercivity spectrum extends to fields at least an order of magnitude higher. Sample HH-2 with a particle size of 0.25  $\mu\text{m}$  has the highest coercive force,  $H_c = 668$  mT. Shape

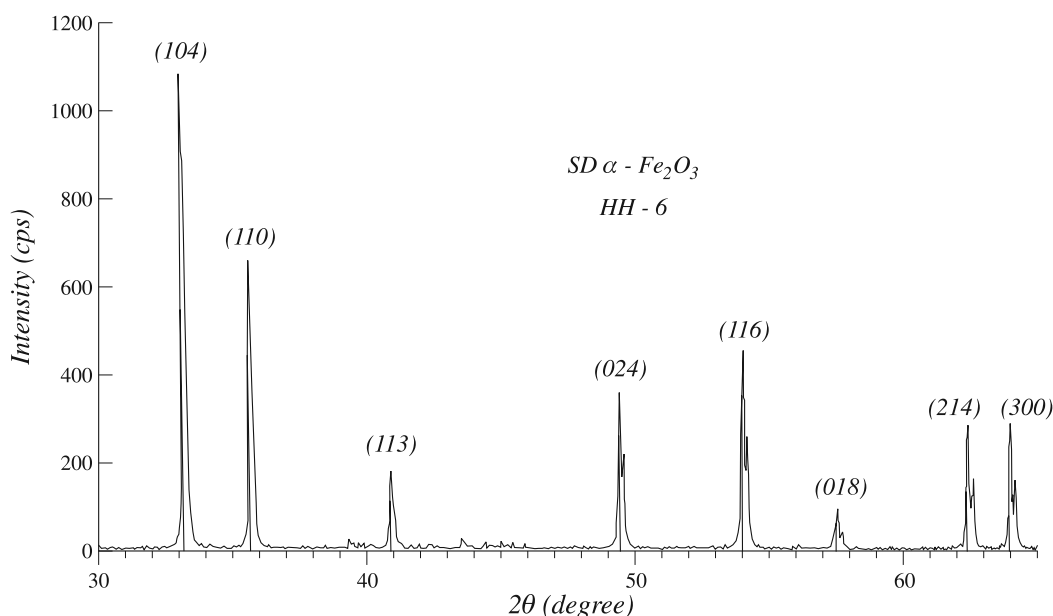


**Figure 1.** X-ray powder diffraction pattern for synthetic hematite HH-6. The reflections are characteristic of hematite; no iron-bearing impurities are detected.

and *c* plane magnetocrystalline anisotropies are inadequate to explain these high coercivities. Their main source must be magnetoelastic anisotropy arising from internal stresses [Porath, 1968].

[13] Remanence ratios  $M_{rs}/M$  for all but two of the SD hematites range from 0.605 to 0.715, intermediate between the random orientation values of 0.5–0.637 for uniaxial (magnetoelastic) anisotropy with an easy plane and 0.75–0.955 for triaxial (magnetocrystalline) anisotropy with an easy plane [Dunlop and Özdemir, 1997, p. 321]. Exceptions are HH-2 with  $M_{rs}/M = 0.805$  and acicular hematite HLP produced from lepidocrocite with  $M_{rs}/M = 0.5$ .

[14] Hysteresis was measured in the (0001) plane for the large single crystals. The loops closed in fields of a few hundred mT (Figure 5).  $H_c$  values were between 0.63 and 30.4 mT, an order of magnitude lower than SD values, although the coercivity spectrum again tailed upward to values much higher than  $H_c$ . Coercivity is determined by the motion of pinned domain walls and is much lower than in the SD hematites where domains must be bodily rotated. Walls are usually pinned at crystal defects such as multiple twins or dislocations [Porath and Raleigh, 1967]. Values of  $H_c$  ranged from 8.1 to 22.4 mT for QC subsamples, indicating that the defects are distributed inhomogeneously. Saturation remanence ratios  $M_{rs}/M_s$  are 0.605–0.895, higher than for the SD hematites because measurements are made within the (0001) easy plane.

### 3. Low-Temperature Cycling of SIRM

[15] Low-temperature magnetization measurements were made with a Quantum Design MPMS2 SQUID magnetometer. Three types of experiments were performed. For type I, samples were given an SIRM in a field of 2.5 T at room temperature (300 K), then cooled to 20 K and warmed back to 300 K in zero field. For type II, the SIRM memory was cooled to 20 K and back to 300 K in zero field. For type III, samples

were given an SIRM in a field of 2.5 T at 20 K, then warmed to 300 K in zero field.

[16] The usual order of experiments for the large MD hematite crystals was I → II → III, but for QC-6 the sequence was III → II → I, and for ELBA-1, the sequence was I → III → II. In these two cases, the “memory” cycled in experiment II was the 20-K SIRM, starting from 300 K after its first passage through  $T_M$  (not really a memory because it was not cycled down as well as up through  $T_M$ ). The sequence was varied in order to see the effect on the amplification of the low-temperature defect magnetization when it was heated above  $T_M$ . There was indeed an effect and 1/3 of the 15 synthetic hematites were run in each of the sequences I → II → III, III → II → I, and I → III → II (see section 3.2).

#### 3.1. Experiments on MD Hematites

[17] The natural single crystals were carefully oriented in the MPMS sample holder so that the (axial) field of the

**Table 2.** Low-Temperature Magnetic Properties of Natural Single Crystals

Sample	<i>d</i> , mm	$T_M$ , K	$R_{SIRM}$	$M_{defect}$ , kA/m
QC-1	0.4 × 2.85 × 4.95	252	0.398	0.0377
QC-2	0.35 × 1.2 × 2.1	250	0.438	0.0339
QC-3	0.3 × 1.1 × 2	254	0.381	0.0187
QC-4	0.4 × 1.8 × 3.7	252	0.385	0.0278
QC-5	0.24 × 2.15 × 3.2	252	0.44	0.044
QC-6	0.35 × 2.9 × 5	250	0.42	0.0356
QC-7	0.2 × 1.2 × 2.1	255	0.36	0.0324
QC-8	0.14 × 1.2 × 1.95	256	0.329	0.0178
QC-9	0.2 × 2.5 × 3.95	253	0.419	0.020
QC-10	0.18 × 2.4 × 3.3	255	0.337	0.0183
QC-11	0.3 × 1.4 × 2.5	258	0.385	0.014
ELBA-1	1 × 3.7 × 5.5	257	0.649	0.061
ELBA-2	0.2 × 1.3 × 1.7	255	0.429	0.024
ELBA-3	0.75 × 2.4 × 3	256	0.639	0.07
BRZ-1	0.4 × 3.2 × 4.5	261	0.172	0.0018
BRZ-2	10 × 600 μm (powder)	259	0.136	0.0029

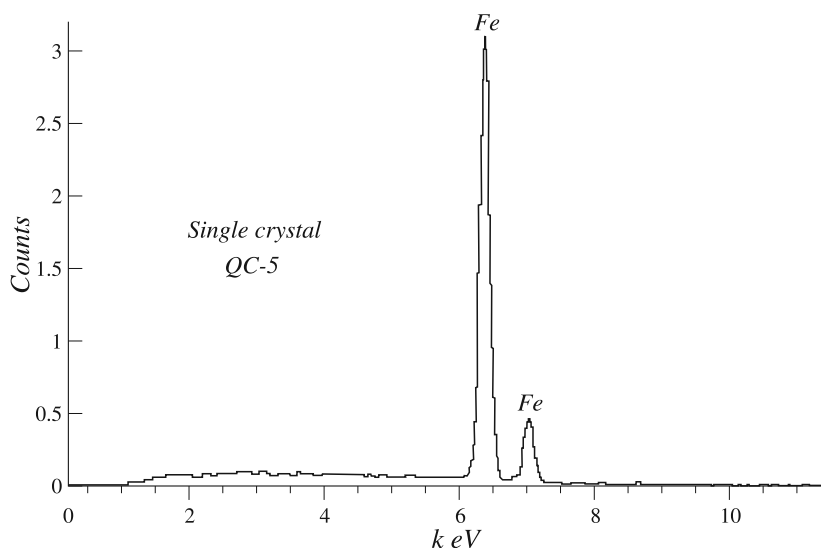


**Figure 2.** X-ray energy dispersive analysis for Quebec hematite crystal QC-5.

superconducting solenoid was in the (0001) plane of the crystal. SIRMs were therefore produced parallel to an easy axis in the basal plane.

[18] Cooling and warming curves of 300-K SIRM for sample QC-5 are shown in Figure 6. From 300 to 270 K, the remanence was independent of  $T$ . As a result of crossing the Morin transition (from 260 to 250 K for QC-5), 98% of the remanence was lost with the disappearance of spin canting. Although the bulk of the crystal underwent the transition, a small fraction of the spins seemingly still lay in the  $c$  plane and did not flop to the antiferromagnetic  $c$  axis. In further cooling, the remanence remained essentially constant below 200 K. The remanence  $M_{20}$  at 20 K, which we take to represent the defect magnetization  $M_d$ , was 0.044 kA/m ( $\text{emu}/\text{cm}^3$ ), 2% of the original 300-K SIRM. On passing again through the Morin transition ( $T_M \approx 255\text{--}265$  K in warming), a sharp

increase in remanence marked the onset of spin canting and resulting basal plane ferromagnetism. The recovered SIRM at room temperature was 44% of the original SIRM, a memory ratio  $R_{\text{SIRM}} = 0.44$ .

[19] In cooling from 300 K to  $T_M$ , the remanence of the other Quebec crystals decreased in much the same way as QC-5. The memory ratios  $R_{\text{SIRM}}$  and defect moments  $M_d$  range from 0.33 to 0.44 and 0.014 to 0.038 kA/m, respectively. Elba hematites have significantly higher memory ratios and defect moments than the Quebec crystals (Table 2).

[20] Brazilian hematites have lower magnetic memories than the other crystals (0.17 and 0.14 for BRZ-1 and -2) and very small defect moments (2–3 A/m). Their spin-flop transitions were very sharp and occurred at 261 and 259 K, respectively. These values are very close to  $T_M = 262\text{--}263$  K

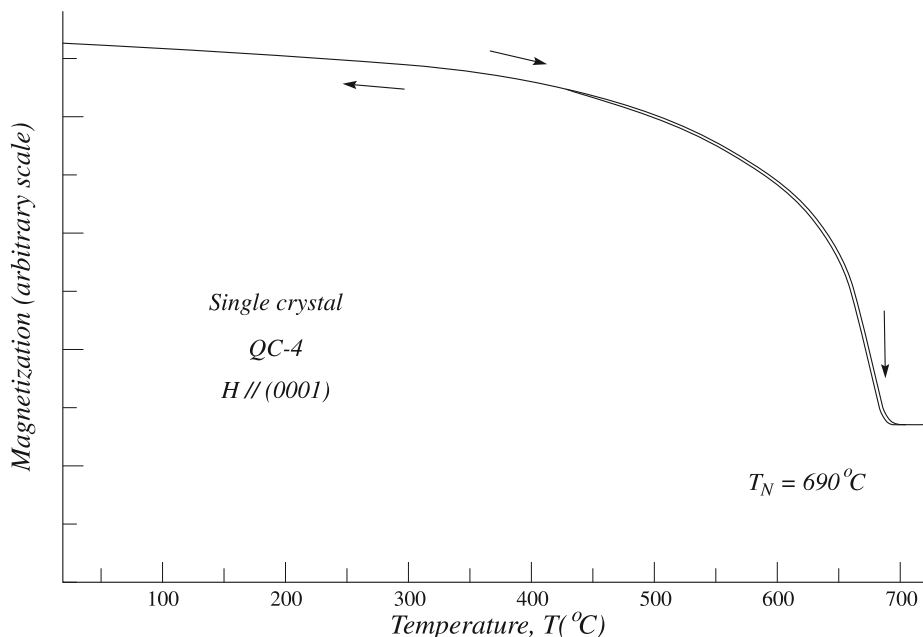


**Figure 3.** Reversible  $M_s$ - $T$  curve of Quebec single crystal QC-4, showing a  $690^\circ\text{C}$  Néel temperature characteristic of hematite.

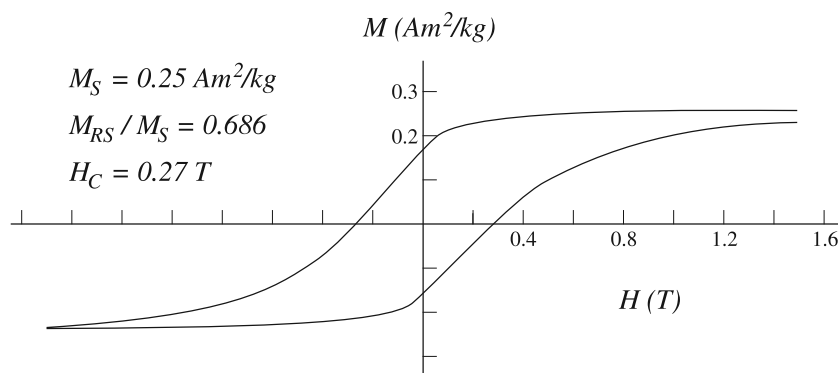


**Figure 4.** Room temperature hysteresis curve of single-domain sample HH-6. Coercivities are very high, and the loop does not close in 1.5 T.

measured for “pure” hematite crystals [Flanders and Remeika, 1965; Besser *et al.*, 1967].

[21] Like other natural hematites, our crystals exhibit a thermal hysteresis in the Morin transition,  $T_M$  being higher in warming than in cooling (Figure 6). For the same cooling/warming rate, the hysteresis is larger in some samples than in others. For example, the hysteresis width  $\Delta T_M$  tends to be smaller in MD crystals than submicron hematites.

[22] Figure 7 shows the results of experiment III, in which crystal QC-5 was cooled to 20 K in zero field, where it was given a new 2.5 T SIRM in the (0001) plane, then warmed in zero field to 300 K and cooled back to 20 K. (Experiment II, cycling the memory of the 300-K SIRM, did not produce any significant remanence change. Before beginning experiment III, the sample in its plastic holder was removed from the MPMS and AF demagnetized, erasing most of the memory.) Although the hematite is nominally in a purely antiferromagnetic state at 20 K, the SIRM is sizable:  $M_{20} = 0.0552 \text{ kA/m}$ . This is close to the value  $M_{20} = 0.044 \text{ kA/m}$  remaining when the 300-K SIRM was zero field cooled to 20 K. Either one is an acceptable estimate of the defect magnetization.

[23] In warming from 20 K, the SIRM remained essentially constant up to 200 K (Figure 7). The Morin transition is sharply defined ( $T_M = 253 \text{ K}$ ). Above  $T_M$  the remanence was 0.72 kA/m, 13 times larger than the low-temperature moment  $M_{20}$  at 20 K. The comparative amplification factor between the 300-K SIRM memory and its corresponding  $M_{20}$  was 18 (Figure 6).

[24] The cooling curve of 20-K SIRM did not exactly retrace the cooling curve but increased slightly between 300 and 260 K. There was no thermal hysteresis at  $T_M$ , and the remanence followed the warming curve in cooling from  $T_M$  to 20 K.

[25] In summary, warming (20 K  $\rightarrow$  300 K) and cooling (300 K  $\rightarrow$  20 K) cycles of low-temperature SIRM (Figure 7) have two important features:

[26] 1. Remanence produced in a demagnetized sample below  $T_M$  (Figure 7) and room temperature remanence that has been cooled through  $T_M$  (Figure 6) increase in identical ways on warming through the Morin transition. The defect moments at 20 K have similar intensities (0.055 and 0.044 kA/m) and so have the SIRM memories at 300 K (0.72 and 0.79 kA/m). In addition, the 20-K SIRM warming curve (Figure 7) and the 300-K SIRM warming half cycle (Figure 6) exhibit similar sharp transitions with identical  $T_M$

of 253 K (determined by extrapolating the linear part of the remanence increase at the transition to intersect the  $T$  axis).

[27] 2. Thermal hysteresis of the Morin transition varies with experimental conditions for the same hematite. In Figure 6 (cooling followed by heating)  $\Delta T_M$  was  $\approx 5 \text{ K}$ , while in Figure 7 (heating followed by cooling)  $\Delta T_M$  was essentially zero, giving a better estimate of  $T_M$ .

### 3.2. Experiments on SD Hematites

[28] Low-temperature cycling of 300-K SIRM for the synthetic SD hematites gave results very similar to those for MD crystals. Results for HH-6 (0.42  $\mu\text{m}$ ) are typical (Figure 8). A large fraction of the initial SIRM demagnetized at  $T_M$  with the disappearance of spin canting. The low-temperature remanence or defect moment which survives below  $T_M$  is  $\approx 2\%$  of the 300-K SIRM and is constant between 200 and 20 K. During the warming half cycle, about one third of the initial remanence was recovered, indicating a similar efficiency of coupling between the defect moment and the spin-canted moment in warming through  $T_M$  for both MD and SD grains.

[29] All the fine grained hematites showed well-defined Morin transitions with  $T_M$  between 228 and 254 K (Table 1). These values are less than the 250–261 K observed for natural single crystals (Table 2). Fine particle size and associated higher internal strains are known to lower  $T_M$  [Nininger and Schroer, 1978; Muench *et al.*, 1985; Zysler *et al.*, 2003], while annealing out internal strain increases  $T_M$  [Suber *et al.*, 1999; Vasquez Mansilla *et al.*, 2002].

[30] As with the MD crystals, the Morin transition of our SD hematites has a thermal hysteresis, with different values of  $T_M$  in cooling and warming cycles. Hysteresis of  $T_M$  is a well-known property of hematite [Lin, 1960; Nininger and Schroer, 1978; Vlasov *et al.*, 1986; Goya *et al.*, 2005]. Chow and Keffer [1974] suggested that magnons at the surface (where the spin rotation initiates) soften differently as  $T_M$  is approached from below or above, depending on the local

**Table 3.** Magnetic Properties of Hematites

Parameters	SD Hematites	MD Hematites
$M_S$ , A m <sup>2</sup> /kg	0.234–0.33	0.31–0.38
$M_{RS}/M_S$	0.50–0.805	0.605–0.895
$\mu_0 H_c$ , mT	140–668	0.9–30.4
$H_{cr}/H_c$	–	1.043–1.17
$T_M$ , K	228–255	250–261
$T_N$ , °C	685–696	679–690

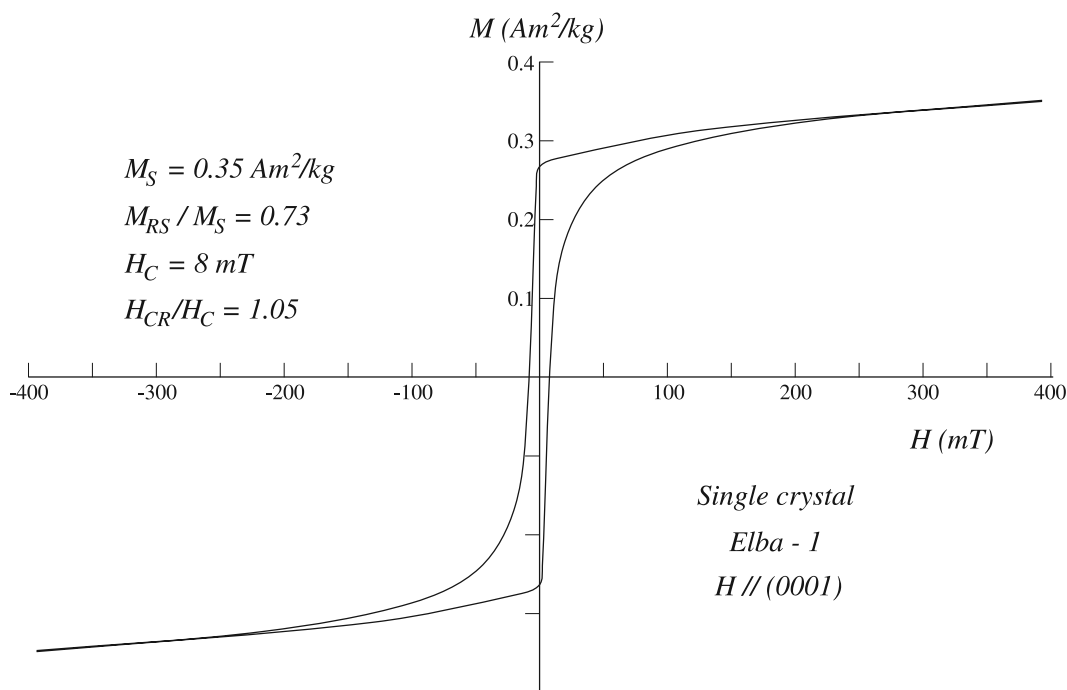


**Figure 5.** Room temperature hysteresis curve of multidomain crystal Elba-1. Coercivities are 1–2 orders of magnitude lower than for single-domain hematite (Figure 4).

surface anisotropy. The spins in these surface regions turn and serve as nucleation centers that generate the transition throughout the crystal interior, the transition occurring when the free energies of the antiferromagnetic (uncanted) and weakly ferromagnetic (spin canted) states are equal.

[31] Figure 9 illustrates experiments II and III from a I  $\rightarrow$  II  $\rightarrow$  III sequence for sample HH-2 (0.25  $\mu\text{m}$ ). Cycling of the memory of 300-K SIRM gives perfectly reversible results, apart from a thermal hysteresis  $\Delta T_M$  of 4–5 K. The transition

extends over a broad region of  $\approx 25$  K. There is no further net loss of remanence in a second cycle through  $T_M$ : the memory regained in the second warming through the transition is identical to the memory after the original cycle (points 1 and 3 in Figure 9).

[32] The memory of the SD samples could not be erased before beginning experiment III because coercivities are higher than the maximum AF demagnetizer field; furthermore, the powdered samples cannot be removed from their

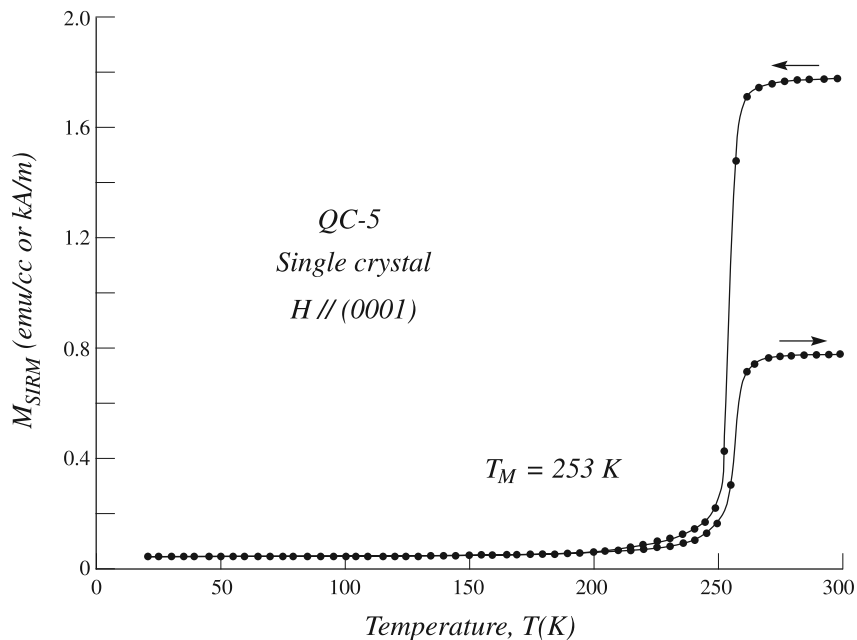


**Figure 6.** Results of experiment I (zero-field cooling and warming of 300-K SIRM) for multidomain hematite crystal QC-5. The memory after cycling is about 45% of the initial SIRM. Thermal hysteresis is evident:  $T_M$  is lower in cooling than in warming through the Morin transition.

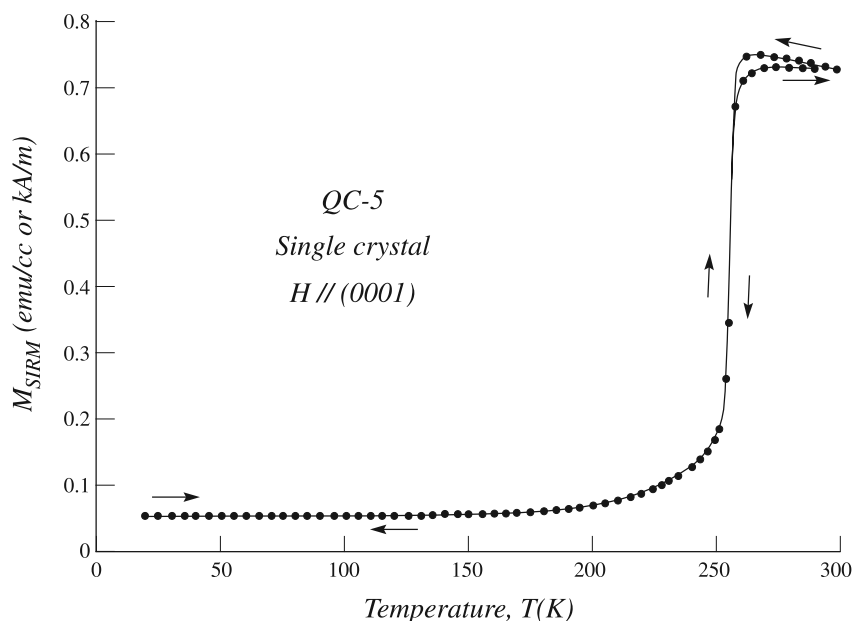


**Figure 7.** Results of experiment III (zero-field warming and cooling of 20-K SIRM) for multidomain crystal QC-5. Unlike the results of cycling 300-K SIRM (Figure 6), the temperature variation is almost reversible. Note that the small 20-K SIRM is greatly amplified on warming through  $T_M$ .

plastic holders for thermal demagnetization. The 20-K SIRM (point 4 in Figure 9) is only slightly higher than the memory moment below  $T_M$  (point 2). The remanences behave almost identically in warming through  $T_M$ , apart from a slightly lower amplification factor  $M_{300}/M_{20}$  (10 for the 20-K SIRM versus 12 for the 300-K SIRM memory).

[33] The picture changes when the experimental sequence is III  $\rightarrow$  II  $\rightarrow$  I (Figure 10). SIRM produced at 20 K in virgin sample HMN-2 ( $0.45 \mu\text{m}$ ), never previously exposed to strong fields, is  $0.0158 \text{ kA/m}$  (point 1). When warmed in zero field, almost half this remanence is lost before the onset of the Morin transition around 250 K, above which the remanence jumps to  $0.070 \text{ kA/m}$  (point 2). In cooling, there is a pronounced thermal hysteresis ( $\Delta T_M = 15\text{--}20 \text{ K}$ ) and below  $T_M$  the remanence is almost flat from 220 to 20 K, with a much reduced intensity:  $0.0038 \text{ kA/m}$  at 20 K. Completing experiment II, the warming half cycle (points 3 to 4) tracks back reversibly until 220 K, rises beginning around 250 K, and finishes about 20% lower than at the beginning of the cycle.

[34] Experiment I is shown only in part in Figure 10. Following SIRM production at 300 K and zero-field cooling to 20 K, the warming half cycle beginning at point 5 rises steeply at a transition temperature much lower than those seen in the experiment III and II warming curves. The remanence ultimately levels out at a 300-K SIRM memory  $M_{300} = 0.353 \text{ kA/m}$ , five times higher than  $M_{300}$  for the 20-K SIRM (point 2).

[35] In summary, when 20-K SIRM is produced first and 300-K SIRM later, we observe two significant differences compared to previous results:

[36] 1. The low-temperature moment decays below  $T_M$  during warming and decreases still further in recooling through  $T_M$ .

[37] 2. The amplification factor of spin-canted/defect magnetization is different in experiment III ( $M_{300}/M_{20} =$

4.5 or 18, depending on whether point 1 or 3 is taken as  $M_{20}$ ) and the subsequent experiment I ( $M_{300}/M_{20} = 21$ ).

[38] In addition, it may be significant that the onset of the Morin transition during warming was much lower in experiment I than in experiment III.

## 4. Discussion

### 4.1. Defect Magnetization and Memory

[39] Despite their different grain sizes and morphologies, defect densities and internal strains, our submicron hematites and large natural crystals had remarkably similar low-temperature cycling curves. Remanence loss at the Morin

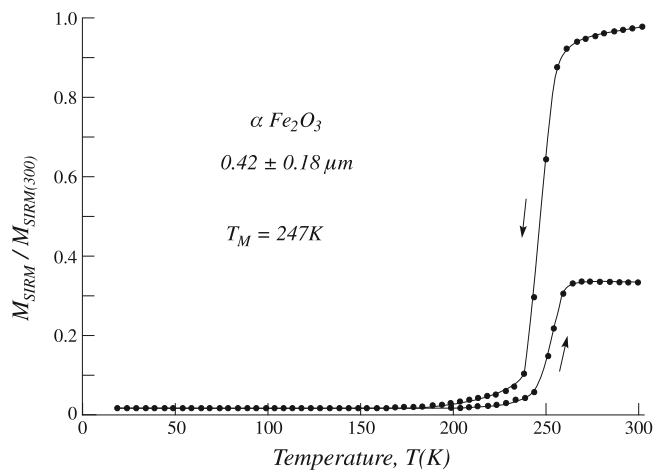


**Figure 8.** Results of experiment I (zero-field cooling and warming of 300-K SIRM) for single-domain hematite sample HH-6 ( $d_{av} = 0.42 \mu\text{m}$ ). The results are very similar to those for multidomain crystals (Figure 6) except for a slightly lower memory ( $R_{\text{SIRM}} = 0.35$ ) and greater thermal hysteresis.

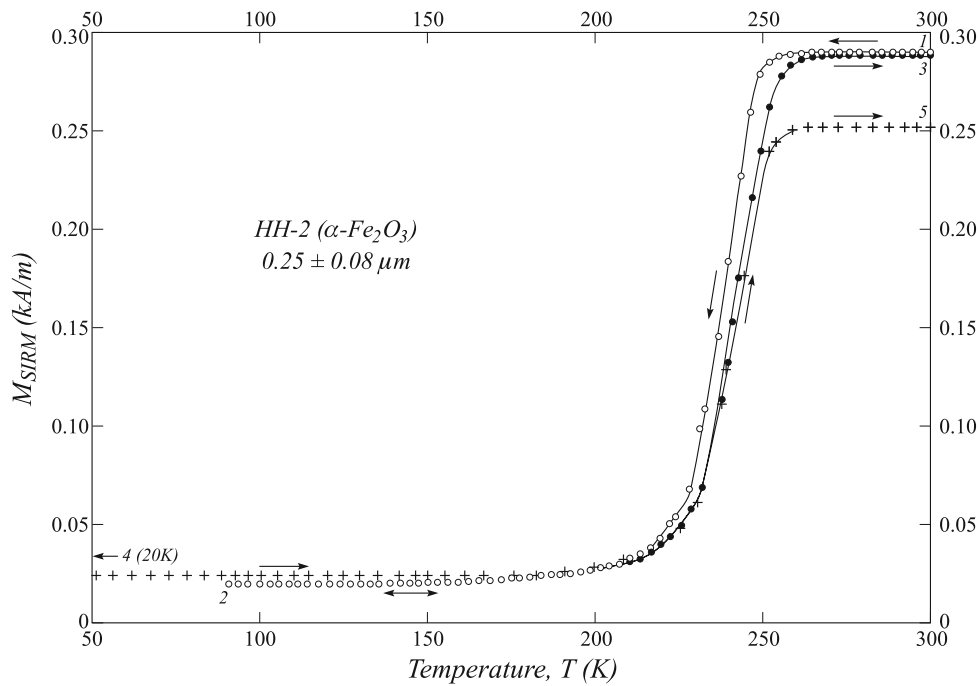


**Figure 9.** Results of experiment II (zero-field cooling and warming of 300-K SIRM memory: 1 → 2 → 3) followed by experiment III (zero-field warming of 20-K SIRM: 4 → 5) for single-domain hematite sample HH-2 ( $d_{av} = 0.25 \mu\text{m}$ ). The amplification factor  $M_{300}/M_{20}$  is 20% higher for 300-K SIRM memory than for 20-K SIRM, but the curves are otherwise similar.

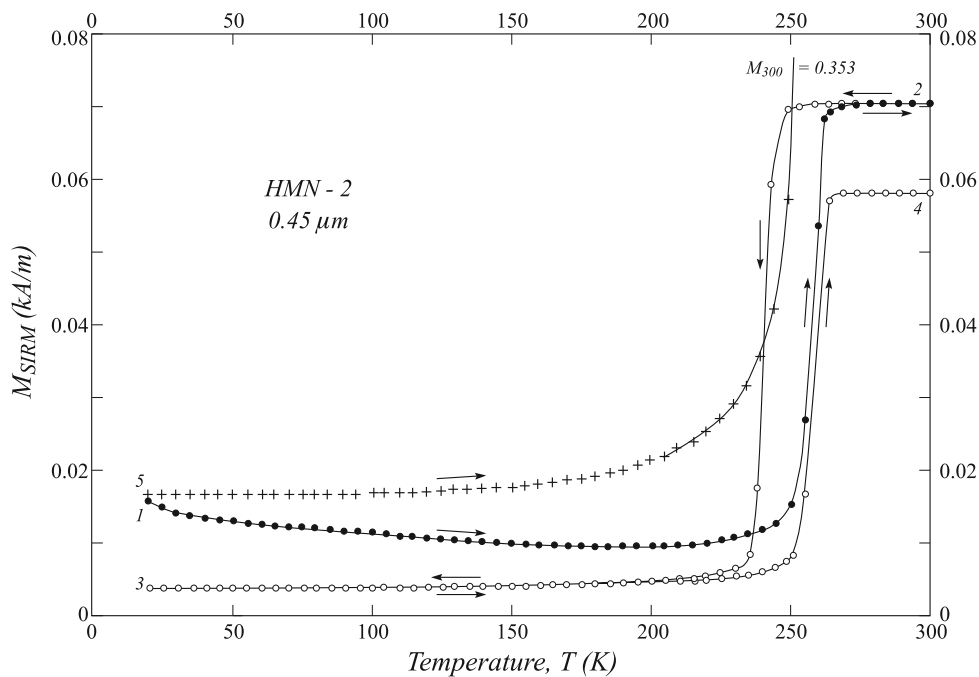


**Figure 10.** Results of the experimental sequence III (cycling of 20-K SIRM: 1 → 2 → 3), followed by II (warming of 20-K SIRM memory), followed by I (cycling of 300-K SIRM: only the warming curve, from 5 onward, is shown). Starting with 20-K SIRM in a virgin sample, results differ from those in Figures 6–9. The warming and cooling curves of 20-K SIRM are distinctly different and there is irreversible loss of remanence on recooling through  $T_M$ . The amplification factor  $M_{300}/M_{20}$  is much higher for 300-K SIRM than for 20-K SIRM.

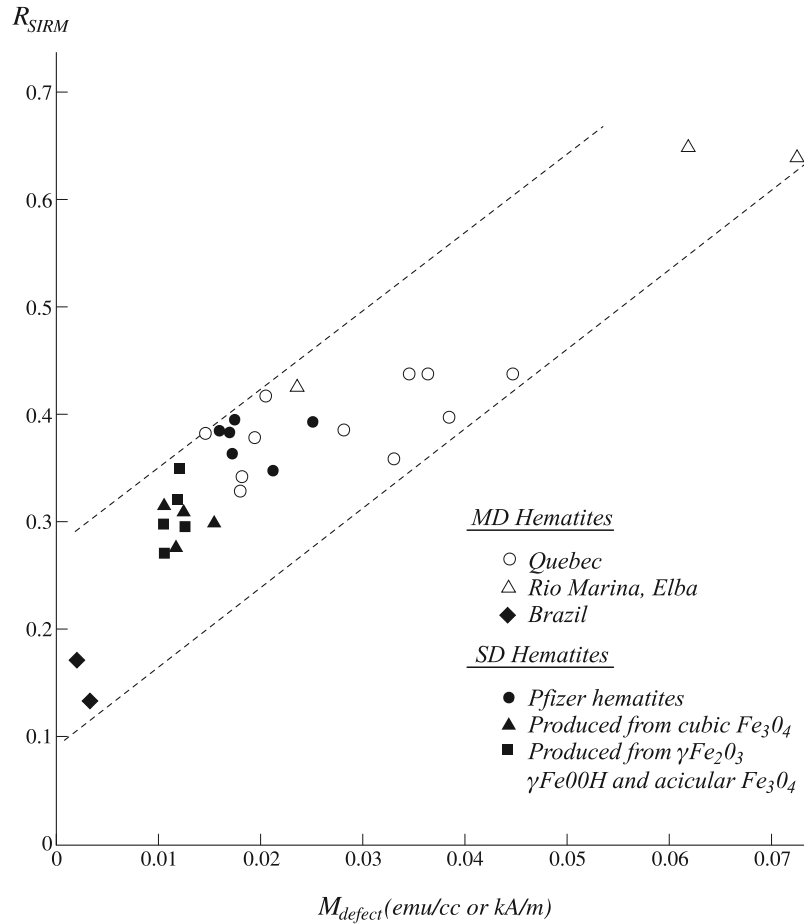


**Figure 11.** Correlation between the memory ratio  $R_{SIRM}$  and the defect magnetization  $M_{defect}$  (the value of 300-K SIRM, measured at 20 K). Larger defect moments below  $T_M$  produce larger spin-canted moments above  $T_M$ .

transition, defect moment below  $T_M$ , and SIRM memory at room temperature were quantitatively similar in all samples. These facts suggest that in SD and MD hematites alike, the small defect remanence that survives cooling through  $T_M$  is responsible for re-nucleating the “memory” spin-canted remanence during warming through  $T_M$ . The universality of its role as a “catalyst” in regenerating the memory implies that the defect magnetization is related to a fundamental material property rather than a particular facet of domain structure. The presence or absence of domain walls seems not to affect the memory in any obvious way.

[40] Figure 11 compares values of the memory ratio  $R_{SIRM}$  and the defect magnetization  $M_{defect} = M_{20}$ , both measured for 300-K SIRM, in submicron and millimeter size crystals. If our hypothesis that the defect moment is responsible for memory is correct, we would expect to see a correlation between  $R_{SIRM}$  and  $M_{defect}$ . This is indeed the case: higher SIRM memory ratios are associated with higher defect moments. The eye is guided by the data for the Brazil and Elba crystals, which have unusually low and high defect moments, respectively, but there is enough variation in  $M_{defect}$  in the other samples to confirm the trend. The synthetic SD hematites on average have somewhat lower  $M_{defect}$  (and  $R_{SIRM}$ ) values than the Québec MD crystals but the range of both parameters is quite narrow considering the

profound differences in domain structure and type of defects between the two groups.

[41] The main sources of defects in submicron hematites are internal strains arising from fine particle size. As the size of nanoparticles decreases, surface to volume ratio increases and surface effects come to dominate the magnetic properties [Hansen *et al.*, 2000]. The structure is modified near the surface, resulting in lower lattice symmetry and broken bonds and giving rise to surface spin disordering [Krishnan *et al.*, 2006]. The surface of a fine particle acts like a large defect, capable of pinning spins and thus affecting magnetic properties [Kündig *et al.*, 1966; Nininger and Schroer, 1978]. Our SD crystals are rather large to be dominated by surface effects. Dislocations in their interiors likely have at least a comparable effect.

[42] In large natural hematite crystals, growth and deformational twinning [Sunagawa and Flanders, 1965; Putnis, 1992], twin boundaries [Porath and Raleigh, 1967] and dislocations [Sunagawa, 1960] are the commonest crystal defects. Other possible defects in natural hematites are voids, nonmagnetic inclusions, and misoriented crystals. These defects introduce a stress-strain distribution to which the ferromagnetic moment couples magnetoelastically. X-ray topography studies of the weakly ferromagnetic phase indicate strong domain wall pinning by twin boundaries, which

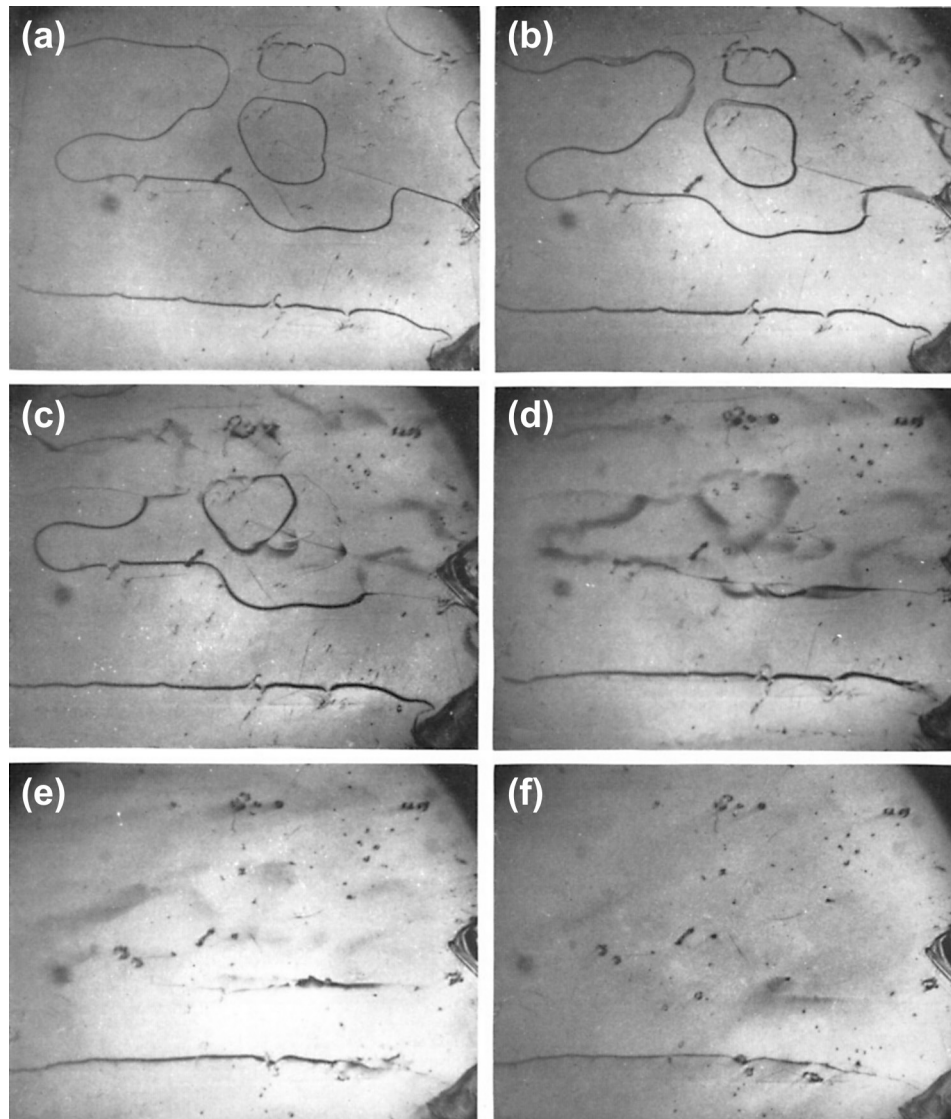


**Figure 12.** Domain patterns observed on a single crystal of hematite above and below the Morin transition [after *Gallon, 1968a*] (with permission from Royal Society London): (a)  $-11.5^{\circ}\text{C}$  (261.5 K); (b)  $-11.7^{\circ}\text{C}$  (261.3 K); (c)  $-11.9^{\circ}\text{C}$  (261.1 K); (d)  $-12.2^{\circ}\text{C}$  (260.8 K); (e)  $-12.5^{\circ}\text{C}$  (260.5 K); (f)  $-13.0^{\circ}\text{C}$  (260 K). Magnification is 17X.

are regions of high strain [*Clark et al., 1983*]. Domain walls pinned by inversion twin boundaries lead to the wall being tilted out of the basal plane [*Tanner et al., 1988*]. Nuclear magnetic resonance studies confirm that a large fraction of  $180^{\circ}$  domains walls are strongly pinned at localized strains [*Hirai et al., 1971; Searle et al., 1972*].

[43] Among these varied mechanisms for lattice defect–magnetization interaction, there are no obvious clues to the fundamental nature of hematite’s defect moment or the reason why it has a similar effect on SD and MD memory. We note in passing that there is direct observational evidence that all memory of the weakly ferromagnetic state above  $T_M$  is not lost below  $T_M$ . Figure 12 shows images of the domain structure in a hematite crystal viewed during cooling through the transition (261.5 K to 260 K) [*Gallon, 1968a*]. The domain boundaries rapidly lose contrast but

shadow images remain in (e) and (f) showing that part at least of the domain structure remains in place.

[44] Figure 13 is a possible model of defect magnetization. We hypothesize that small regions of spins pinned to crystal defects resist the general tendency to rotate to the  $c$  axis during cooling through  $T_M$ . Magnetoelastic coupling between spins and crystal imperfections is strong in hematite but probably not so powerful as to hold the spins in the basal plane. Nevertheless, because our measurements are made in the basal plane, the pinned spins must have a net component in that plane, presumably oriented along the same easy axis they favored above  $T_M$ . On rewarming through  $T_M$ , this spin nucleus serves to reorient the moment of an entire SD grain. In MD grains, where there are multiple defects and spin nuclei, an approximation to the previous domain pattern will be renucleated around these specific sites, as is observed in domain images taken during warming. The defect moment

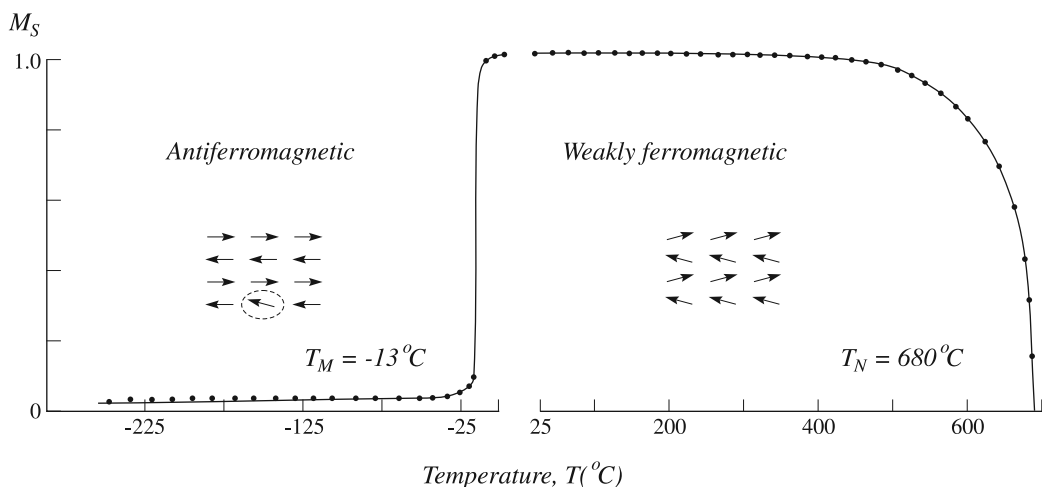


**Figure 13.** Schematic diagram of our model for the defect magnetization. Above  $T_M$ , spins lie in the basal plane and are canted, leading to weak ferromagnetism. Below  $T_M$ , most spins are aligned with the  $c$  axis in perfect antiferromagnetism, except for isolated clusters of spins (circled) which are pulled out of alignment by magnetoelastic interaction with crystal defects. These can be reoriented azimuthally by a strong field to give an SIRM at very low  $T$ . They also act as nuclei for producing spin-canted magnetization in the same direction within the basal plane above  $T_M$ .

we imagine in our model forms an integral unit with the spin-canted magnetization above  $T_M$ , all spins lying in the  $c$  plane. Even below  $T_M$ , exchange coupling cannot be broken and the defect region's spins must lie much closer to the  $c$  axis than the basal plane, explaining why the low-temperature moment below  $T_M$  is only a few percent of the weak ferromagnetism above  $T_M$ .

#### 4.2. Defect–Spin-Canted Coupling

[45] Our model gives a first-order picture of memory across the Morin transition but leaves unanswered the question of why memory ratios  $R_{\text{SIRM}}$  are so similar in SD and MD grains. No coupling mechanism is perfect and it is natural that some SD grains should renucleate their moments in a different easy direction after rewarming. Likewise it is understandable that domain structure will lose some of its fine detail in cycling through  $T_M$  (although the details seem to be well preserved in a second cycling). However, why the fraction of SD grains that remember their original easy axis, as measured by  $R_{\text{SIRM}}$ , should so closely match the fraction of remanence preserved by domain wall displacements in an average MD grain is unclear.

[46] The efficiency of memory indicated by  $R_{\text{SIRM}}$  clearly increases with increasing size of the spin cluster and/or angle of spin deflection away from the  $c$  axis, as measured by  $M_{\text{defect}}$  (Figure 11). We found that the SIRM produced at 20 K,  $M_{20}$ , was similar in intensity to  $M_{\text{defect}}$  (for which we used the 20 K value of SIRM produced at 300 K) for about 3/4 of the samples.  $M_{20}$  would be an equally acceptable estimate of the defect moment for these samples.

[47] It is not at first sight obvious why these two measures should be similar in intensity. The 300-K SIRM is produced in the weakly ferromagnetic region where all spins lie in the basal plane. The 2.5 T field only has to work against basal plane anisotropy. At 20 K, most spins are pinned along the  $c$  axis by a much stronger anisotropy, against which 2.5 T has a negligible effect. So how is 20-K

SIRM produced? Our model has the spin clusters that represent the defect magnetization tilted away from the  $c$  axis (Figure 13). They are free to rotate about the  $c$  axis and will do so against the basal plane anisotropy, which we conclude must be similar in the antiferromagnetic region below  $T_M$  to its value at 300 K. Basal plane anisotropy has not been measured below  $T_M$  to our knowledge. At the Morin transition, the spins flop because the anisotropy between the  $c$  axis and the  $c$  plane changes sign, but there is no reason to expect that the much weaker anisotropy within the  $c$  plane is correlated in its  $T$  dependence with the  $c$  axis anisotropy. In the titanomagnetites, for example, the anisotropy constants  $K_1$  and  $K_2$  have totally different  $T$  variations.

[48] Having established that for the majority of our hematites, the defect moment is similar whether it is manifested by a 300-K SIRM that has been “cleaned” of its spin-canted moment by cooling through  $T_M$  or by an SIRM produced at 20 K in the absence of any spin-canted moment, we come to another question. If these two defect magnetizations are really equivalent (both representing pinning along some preferred axis in the basal plane), then in warming through  $T_M$  both should nucleate/renucleate similar magnetizations at ordinary temperatures. In other words, the ratio  $M_{300}/M_{20}$  should be comparable in the two cases. For some samples this is so, but for others it is not. For example, QC-5 has  $M_{300}/M_{20} = 18$  for the memory of 300-K SIRM and  $M_{300}/M_{20} = 13$  for 20-K SIRM (Figures 6 and 7). For HMN-2 (Figure 10),  $M_{300}/M_{20} = 21$  for 300-K SIRM memory and either 4.5 or 18 for 20-K SIRM, depending on whether the virgin intensity or the value after cycling up and down through  $T_M$  is used as  $M_{20}$ .

[49] The example of HMN-2 raises another question. Why does the virgin 20-K SIRM lose almost 40% of its intensity during warming from 20 to 200 K, and a further 35% on the return cooling through  $T_M$ ? If the defect magnetization is simply a group of spins magnetoelastically coupled to an

unchanging lattice defect, how can it change in either warming or cooling? When 300-K SIRM is cooled through  $T_M$ , the remanence is perfectly flat and reversible in its  $T$  variation from 200 to 20 K and back again, as is the 20-K SIRM after it has been cycled through  $T_M$ . Our picture of the low-temperature moment in hematite is evidently too simplistic: an SIRM produced in a virgin sample below  $T_M$  has a fraction that responds to changing  $c$  axis anisotropy, particularly the appearance and disappearance of spin canting at  $T_M$ . Only when this fraction is stripped away by passage through  $T_M$  is the part governed by basal plane anisotropy revealed.

## 5. Conclusions

[50] This study of a large collection of natural MD hematite crystals and synthetic submicron SD hematites reveals features not evident in earlier observations. Low-temperature cycling of 300-K and 20-K SIRMs of one large single crystal [Özdemir and Dunlop, 2005] showed similar spin-canted/defect ratios:  $M_{300}/M_{20} = 20$  and 25, respectively. In the present study, this amplification factor is more variable. Usually (in all but three samples) the ratio is higher for memory of 300-K SIRM than for 20-K SIRM. All ratios fall in the range 10–28 except for four ratios of  $\approx 5$  based on virgin 20-K SIRM. Coupling efficiencies for SD and MD crystals were not significantly different.

[51] There was a clear correlation in our study between the memory ratio  $R_{\text{SIRM}}$  (memory after cycling through  $T_M$ /original SIRM produced at 300 K) and the defect magnetization  $M_{\text{defect}}$  (the 20 K value of the 300-K SIRM, measured after a single passage through  $T_M$ ). This correlation (Figure 11) demonstrates that spin-canted ferromagnetism does not renucleate haphazardly in warming through  $T_M$  but is guided by the defect ferromagnetism present in the antiferromagnetic region below  $T_M$ .

[52] In our model the two are exchange coupled: defect magnetization consists of clusters of spins within the general antiferromagnetic lattice that are magnetoelastically bound to the stress fields of lattice defects. Below  $T_M$  magnetoelastic coupling is strong enough to pull these spins some distance away from the  $c$  axis and preserve a component of magnetization in the basal plane (the plane of measurement for our large single crystals). This component can be reoriented within the basal plane at 20 K by a sufficiently strong field, producing SIRM in a previously demagnetized sample. Although not entirely equivalent to the defect moment produced by cooling a room temperature SIRM (which involves the entire spin lattice) through  $T_M$ , the low-temperature SIRM has a similar capacity for generating a greatly amplified remanence on warming through  $T_M$ .

[53] Judging by the memory ratios  $R$  in Figure 11, the defect–spin-canted coupling is about equally efficient for SD and MD remanences (excluding the Elba and Brazil crystals). In the SD case, a fraction  $R$  of the total population of SD grains regenerates a spin-canted moment in the same easy direction it occupied in the original SIRM, while the other grain moments are reoriented at random: an all-or-nothing outcome. In the MD case, guided by similar spin nuclei pinned to defects, domain walls re-form in approximately but not exactly the pattern they had in the original SIRM (see Figure 12). The fraction of remanence recovered

by different MD grains may vary, but the outcome is not all or nothing: every grain recovers some of its original SIRM, the average recovery being  $R$ .

[54] A final observation is that the Morin transition is quite variable, even among closely related samples.  $T_M$  ranged from 250 to 258 K for the QC crystals (Table 2) and even more widely, from 228 to 254 K, for the more heterogeneous synthetic hematites (Table 1). Fine grains have consistently lower  $T_M$  values, although there is not a 1-1 correlation between grain size and  $T_M$  (Table 1). There is almost always a thermal hysteresis between cooling and warming half cycles,  $\Delta T_M$  varying from essentially zero (Figure 7) to almost 20 K (Figure 11).

[55] **Acknowledgments.** We thank Malcolm Back and Bob Ramik of the Royal Ontario Museum, Toronto, for donating the natural single crystals of hematite and Thelma S. Berquo for the Brazilian powder hematite. Helpful reviews were provided by France Lagroix and an anonymous referee. Hysteresis and low-temperature cycling data were measured at the Institute for Rock Magnetism, University of Minnesota, which is operated with support from the Keck Foundation and the Earth Sciences Division of NSF. We thank Jim Marvin, Mike Jackson, and Peat Sølheid for help with the experiments. This research was supported by NSERC Canada grant A7709 to D.J.D.

## References

- Besser, P. J., A. H. Morrish, and C. W. Searle (1967), Magnetocrystalline anisotropy of pure and doped hematite, *Phys. Rev.*, *153*, 632–640.
- Chevallier, R. (1951), Propriétés magnétiques de l'oxyde ferrique rhomboédrique ( $\text{Fe}_2\text{O}_3\alpha$ ), *J. Phys. Radium*, *12*, 172–188.
- Christensen, P. R., et al. (2004), Mineralogy at Meridiani Planum from the Mini-TES experiment on the Opportunity Rover, *Science*, *306*, 1733–1739.
- Chow, H., and F. Keffer (1974), Soft surface magnons and the first-order magnetic phase transitions in antiferromagnetic hematite, *Phys. Rev.*, *10*, 243–254.
- Clark, G. F., P. A. Goddard, J. R. S. Nicholson, and B. K. Tanner (1983), Evidence for very-large-area magnetic domain walls in haematite ( $\alpha\text{-Fe}_2\text{O}_3$ ), *Philos. Mag.*, *B*, *47*, 307–313.
- Dunlop, D. J. (1971), Magnetic properties of fine-particle hematite, *Ann. Geophys.*, *27*, 269–293.
- Dunlop, D. J., and Ö. Özdemir (1997), *Rock Magnetism: Fundamentals and Frontiers*, 573 pp., Cambridge Univ. Press, New York.
- Dzyaloshinsky, I. (1958), A thermomagnetic theory of “weak” ferromagnetism of antiferromagnetics, *J. Phys. Chem. Solids*, *4*, 241–255.
- Flanders, P. J., and J. P. Remeika (1965), Magnetic properties of hematite single crystals, *Philos. Mag.*, *11*, 1271–1288.
- Freier, S., M. Greenspan, P. Hillman, and H. Shechter (1962), The antiferromagnetic Curie point in  $\alpha\text{-Fe}_2\text{O}_3$ , *Phys. Lett.*, *2*, 191–192.
- Gallon, T. E. (1968a), The ferromagnetic domain structure of haematite, *Proc. R. Soc. London, Ser. A*, *303*, 525–529.
- Gallon, T. E. (1968b), The remanent magnetization of haematite single crystals, *Proc. R. Soc. London, Ser. A*, *303*, 511–524.
- Glotch, T. D., and P. R. Christensen (2005), Geologic and mineralogic mapping of Aram Chaos: Evidence for a water-rich history, *J. Geophys. Res.*, *110*, E09006, doi:10.1029/2004JE002389.
- Goya, G. F., M. Veith, R. Rapalaviciute, H. Shen, and S. Mathur (2005), Thermal hysteresis of spin reorientation at Morin transition in alkoxide derived hematite nanoparticles, *Appl. Phys.*, *80*, 1523–1526.
- Haigh, G. (1957a), The effect of added titanium and aluminum on the magnetic behaviour of  $\alpha$  ferric oxide, *Philos. Mag.*, *2*, 505–520.
- Haigh, G. (1957b), Observation on the magnetic transition in hematite at  $-15^\circ\text{C}$ , *Philos. Mag.*, *2*, 877–890.
- Hansen, M. F., C. B. Koch, and S. Mørup (2000), Magnetic dynamics of weakly and strongly interacting hematite nanoparticles, *Phys. Rev.*, *62*, 1124–1135.
- Hirai, A. J., A. Eaton, and C. W. Searle (1971),  $\text{Fe}^{57}$  nuclear magnetic resonance and some dynamical characteristics of domain walls in  $\alpha\text{-Fe}_2\text{O}_3$ , *Phys. Rev. B*, *3*, 68–75.
- Klingelhöfer, G., et al. (2004), Jarosite and hematite at Meridiani Planum from Opportunity's Mössbauer spectrometer, *Science*, *306*, 1740–1745.
- Krishnan, K. M., et al. (2006), Nanomagnetism and spin electronics: Materials, microstructure and novel properties, *J. Mater. Sci.*, *41*, 793–815.
- Kündig, W., H. Bömmel, G. Constabaris, and R. H. Lindquist (1966), Some properties of supported small  $\alpha\text{-Fe}_2\text{O}_3$  particles determined with the Mössbauer effect, *Phys. Rev.*, *142*, 327–333.

- Lielmezs, J., and A. C. D. Chaklader (1965), Reversible thermal effect in  $\alpha$ -Fe<sub>2</sub>O<sub>3</sub> at 690°C ± 5°C, *J. Appl. Phys.*, *36*, 866.
- Lin, S. T. (1960), Magnetic behaviour in the transition region of a hematite single crystal, *J. Appl. Phys.*, *31*, 273S–274S.
- Moriya, T. (1960), Theory of magnetism of NiF<sub>2</sub>, *Phys. Rev.*, *117*, 635–662.
- Muench, G. J., S. Arajs, and E. Matijević (1985), The Morin transition in small  $\alpha$ -Fe<sub>2</sub>O<sub>3</sub> particles, *Phys. Status Solidi A*, *92*, 187–192.
- Néel, L. (1949), Essai d'interprétation des propriétés magnétiques du sesquioxyde de fer rhomboédrique, *Ann. Phys.*, *4*, 249–268.
- Néel, L. (1953), Some new results on antiferromagnetism and ferromagnetism, *Rev. Mod. Phys.*, *25*, 58–63.
- Néel, L., and R. Pauthenet (1952), Étude thermomagnétique d'un monocristal de Fe<sub>2</sub>O<sub>3</sub> $\alpha$ , *C.R. Acad. Sci.*, *234*, 2172–2174.
- Nininger, R. C., and D. Schroerer (1978), Mössbauer studies of the Morin transition in bulk and microcrystalline  $\alpha$ -Fe<sub>2</sub>O<sub>3</sub>, *J. Phys. Chem. Solids*, *39*, 137–144.
- Özdemir, Ö., and D. J. Dunlop (2005), Thermoremanent magnetization of multidomain hematite, *J. Geophys. Res.*, *110*, B09104, doi:10.1029/2005JB003820.
- Porath, H. (1968), Stress-induced magnetic anisotropy in natural single crystals of hematite, *Philos. Mag.*, *17*, 603–608.
- Porath, H., and C. B. Raleigh (1967), An origin of the triaxial basal-plane anisotropy in hematite crystals, *J. Appl. Phys.*, *38*, 2401–2402.
- Putnis, A. (1992), *Introduction to Mineral Sciences*, 457 pp., Cambridge Univ. Press, New York.
- Searle, C. W., S. Kupca, and J. H. Davis (1972), Nuclear magnetic resonance study of tightly pinned domain walls in  $\alpha$ -Fe<sub>2</sub>O<sub>3</sub>, *Phys. Rev. B*, *5*, 3441–3445.
- Squyres, S. W., and A. H. Knoll (2005), Sedimentary rocks at Meridiani Planum: Origin, diagenesis, and implications for life on Mars, *Earth Planet. Sci. Lett.*, *240*, 1–10.
- Squyres, S.W., et al. (2004), In situ evidence for an ancient aqueous environment at Meridiani Planum, Mars, *Science*, *306*, 1709–1714.
- Suber, L., D. Fiorani, P. Imperatori, S. Foglia, A. Montone, and R. Zysler (1999), Effects of thermal treatments on structural and magnetic properties of acicular  $\alpha$ -Fe<sub>2</sub>O<sub>3</sub> nanoparticles, *Nanostruct. Mater.*, *11*, 797–803.
- Sunagawa, I. (1960), Growth history of hematite, *Am. Mineral.*, *45*, 566–575.
- Sunagawa, I., and P. J. Flanders (1965), Structural and magnetic studies in hematite single crystals, *Philos. Mag.*, *11*, 747–761.
- Tanner, B. K., G. F. Clark, and M. Safa (1988), Domain structures in haematite ( $\alpha$ -Fe<sub>2</sub>O<sub>3</sub>), *Philos. Mag.*, *B*, *57*, 361–377.
- Vasquez Mansilla, M., R. Zysler, D. Fiorani, and L. Suber (2002), Annealing effects on magnetic properties of acicular hematite nanoparticles, *Physica B*, *320*, 206–209.
- Vlasov, K. B., E. A. Rozenberg, V. I. Timoshchuk, and Y. G. Smorodinski (1986), Observation of a thermal hysteresis of the magnetization of a hematite single crystal near Morin transition, *Sov. Phys. Solid State*, *28*, 1851–1853.
- Zysler, R. D., D. Fiorani, A. M. Tesla, L. Suber, E. Agostinelli, and M. Godinho (2003), Size dependence of the spin-flop transition in hematite nanoparticles, *Phys. Rev.*, *68*, 212408.

---

D. J. Dunlop and Ö. Özdemir, Department of Chemical and Physical Sciences, University of Toronto at Mississauga, 3359 Mississauga Road, N., Mississauga, ON, Canada L5L 1C6. (ozdemir@physics.utoronto.ca)